

## RESEARCH ARTICLE

10.1002/2016JC011804

## The spectral albedo of sea ice and salt crusts on the tropical ocean of Snowball Earth: II. Optical modeling

Regina C. Carns<sup>1,2</sup>, Bonnie Light<sup>1</sup>, and Stephen G. Warren<sup>2,3</sup>

## Key Points:

- Optical properties of cold sea ice surfaces with salt crust are simulated using radiative transfer modeling
- Salt crust albedo is high across the spectrum, notably so at near infrared wavelengths owing to small absorption by hydrohalite
- A salt crust albedo parameterization presented for use in climate models is expected to yield critical salt-albedo feedbacks

## Correspondence to:

R. Carns,  
rcarns@uw.edu

## Citation:

Carns, R. C., B. Light, and S. G. Warren (2016), The spectral albedo of sea ice and salt crusts on the tropical ocean of Snowball Earth: II. Optical modeling, *J. Geophys. Res. Oceans*, 121, 5217–5230, doi:10.1002/2016JC011804.

Received 18 MAR 2016

Accepted 7 JUN 2016

Accepted article online 16 JUN 2016

Published online 31 JUL 2016

<sup>1</sup>Polar Science Center, Applied Physics Laboratory, University of Washington, Seattle, Washington, USA, <sup>2</sup>Department of Earth and Space Sciences, University of Washington, Seattle, Washington, USA, <sup>3</sup>Department of Atmospheric Sciences, University of Washington, Seattle, Washington, USA

**Abstract** During the Snowball Earth events of the Neoproterozoic, tropical regions of the ocean could have developed a precipitated salt lag deposit left behind by sublimating sea ice. The major salt would have been hydrohalite, NaCl·2H<sub>2</sub>O. The crystals in such a deposit can be small and highly scattering, resulting in an allwave albedo similar to that of snow. The snow-free sea ice from which such a crust could develop has a lower albedo, around 0.5, so the development of a crust would substantially increase the albedo of tropical regions on Snowball Earth. Hydrohalite crystals are much less absorptive than ice in the near-infrared part of the solar spectrum, so their presence at the surface would increase the overall albedo as well as altering its spectral distribution. In this paper, we use laboratory measurements of the spectral albedo of a hydrohalite lag deposit, in combination with a radiative transfer model, to infer the inherent optical properties of hydrohalite as functions of wavelength. Using this result, we model mixtures of hydrohalite and ice representing both artificially created surfaces in the laboratory and surfaces relevant to Snowball Earth. The model is tested against sequences of laboratory measurements taken during the formation and the dissolution of a lag deposit of hydrohalite. We present a parameterization for the broadband albedo of cold, sublimating sea ice as it forms and evolves a hydrohalite crust, for use in climate models of Snowball Earth.

## 1. Introduction

Thick first-year sea ice has an albedo of 0.4–0.5, rising to 0.7 or higher if it is covered by a layer of snow [Brandt *et al.*, 2005]. Open ocean has an albedo around 0.07 [Payne, 1972; Pegau and Paulson, 2001; Brandt *et al.*, 2005; Zatko and Warren, 2015]. This large albedo contrast between unfrozen and frozen ocean surface, and the corresponding contrast in the amount of solar heating, leads to a positive “ice-albedo feedback.” If the ice cover reaches the subtropics, it can lead to a runaway positive feedback that covers the entire ocean with ice [Budyko, 1969]. Earth is thought to have undergone such a transformation at least twice during the Neoproterozoic, the so-called “Snowball Earth” events [Kirschvink, 1992; Hoffman and Schrag, 2002].

As ocean water freezes, the resulting sea ice traps small inclusions of liquid brine. This brine remains in the ice until summer heating raises the ice temperature above  $-5^{\circ}\text{C}$ ; around this temperature, the interconnections of brine inclusions form a permeable network that allows surface meltwater to flush the brine out of the ice [Golden *et al.*, 1998], leaving it with only trace amounts of salt [e.g., Carns *et al.*, 2015, Figure 4]. It is possible, however, that some or all of the sea ice on Snowball Earth could have remained cold enough to avoid drainage and flushing and retain significant salt [Pierrehumbert *et al.*, 2011].

Surface ice on Snowball Earth could even be cold enough for the salts dissolved in the brine to precipitate. Several different salts are known to precipitate from seawater as it concentrates during freezing. Laboratory studies suggest that ikaite (CaCO<sub>3</sub>·6H<sub>2</sub>O) precipitates at temperatures just below the freezing point of seawater [Hu *et al.*, 2014] and observations in modern sea ice have confirmed its presence [Dieckmann *et al.*, 2008, 2010]. Mirabilite (Na<sub>2</sub>SO<sub>4</sub>·10H<sub>2</sub>O) precipitates around  $-8^{\circ}\text{C}$ , while the most abundant salt in seawater, sodium chloride, precipitates around  $-23^{\circ}\text{C}$  as the dihydrate mineral hydrohalite (NaCl·2H<sub>2</sub>O) [Marion *et al.*, 1999]. Once precipitated, hydrohalite crystals, along with some water ice crystals, occupy most of the volume of the brine inclusion and enhance scattering of incoming light [Perovich and Grenfell, 1981; Light *et al.*, 2003;

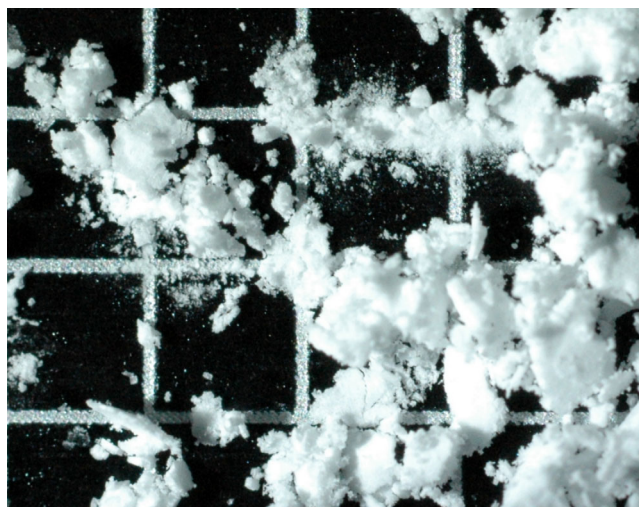


**Figure 1.** Grains of hydrohalite disaggregated from crust. The squares of the grid are 2 mm in width. The crust was fine and powdery and easy to remove from the ice surface.

*Carns et al., 2015*]. Other salts, such as magnesium chloride, keep a small amount of brine liquid until the temperature drops below  $-37^{\circ}\text{C}$  [*Marion et al., 1999*].

In regions of net sublimation on the surface of a Snowball Earth, the ice matrix around these precipitated cryogenites would gradually sublimate away, leaving the salts to form a lag deposit on the surface. Previous work [*Light et al., 2009*] shows that a lag deposit of hydrohalite is highly reflective, suggesting that it could significantly influence the planetary energy balance of Snowball Earth. To quantify this effect, the albedo of an artificially created lag deposit has now been measured in the laboratory [*Carns et al., 2016; Light et al., 2016*]. In this

paper, we use those data, along with radiative transfer modeling, to infer the spectral absorption coefficient of hydrohalite. Using this result along with additional known optical properties of hydrohalite and water ice, we predict the apparent optical properties of cold, sublimating sea ice for scenarios difficult to test in the laboratory.

## 2. Laboratory Measurements

As described in more detail in the companion paper, a hydrohalite (HH) lag deposit was created on a substrate of artificial sea ice in a walk-in freezer laboratory. The sea-ice substrate had been created by filling an insulated 1000 L tank with a solution of NaCl and lowering the temperature to  $-30^{\circ}\text{C}$ . The albedo of this surface was measured during freezing using the method described in *Light et al. [2015]*. The hydrohalite lag deposit was created by spraying a chilled, highly saline solution onto the cold substrate, forming a layer of hydrohalite-rich ice. The end result was a layer consisting of 25% hydrohalite and 75% water ice by volume (assuming a density of  $1.6\text{ g cm}^{-3}$  for hydrohalite [*Adams and Gibson, 1930*] and  $0.92\text{ g cm}^{-3}$  for ice.) We estimated this layer of hydrohalite-rich ice (hereafter referred to as HH-rich ice) to be roughly 2 mm thick. The layer was somewhat irregular, so this thickness represents a source of uncertainty in interpreting our measurements.

Note that, although our primary reason for creating this layer was to reduce the amount of time required for a thick layer of hydrohalite to build up as a lag deposit, it is also analogous to a situation that might occur on Snowball Earth: a melted and refrozen pool of surface brine. Once a lag deposit of salt has built up, temperatures above the dissolution point of the hydrated salt will result in the formation of ponds of saturated brine. When temperatures drop again, the ponds will freeze as a mixture of ice and hydrated salt with a composition similar to that of the layer we created in the laboratory.

After the layer of HH-rich ice was formed, the ice matrix was allowed to sublimate away, leaving behind a layer of small grains of hydrohalite with air filling the space that had previously been occupied by ice. This layer is hereafter referred to as the hydrohalite crust. A sample of the crust material is shown in Figure 1. We measured the albedo of the tank surface periodically as the ice sublimated and the (mostly ice-free) layer of hydrohalite grew thicker. We expected the albedo of this ice-free hydrohalite crust to be higher than that of the HH-rich ice, due to the greater contrast in refractive index between hydrohalite and air versus that between hydrohalite and ice, and this was borne out by observations. We took measurements as the ice continued to sublimate, with initial measurements at 2, 5, and 7 days after applying the HH-rich ice layer, and measurements roughly once per week thereafter. We continued these measurements until the albedo appeared to stabilize.

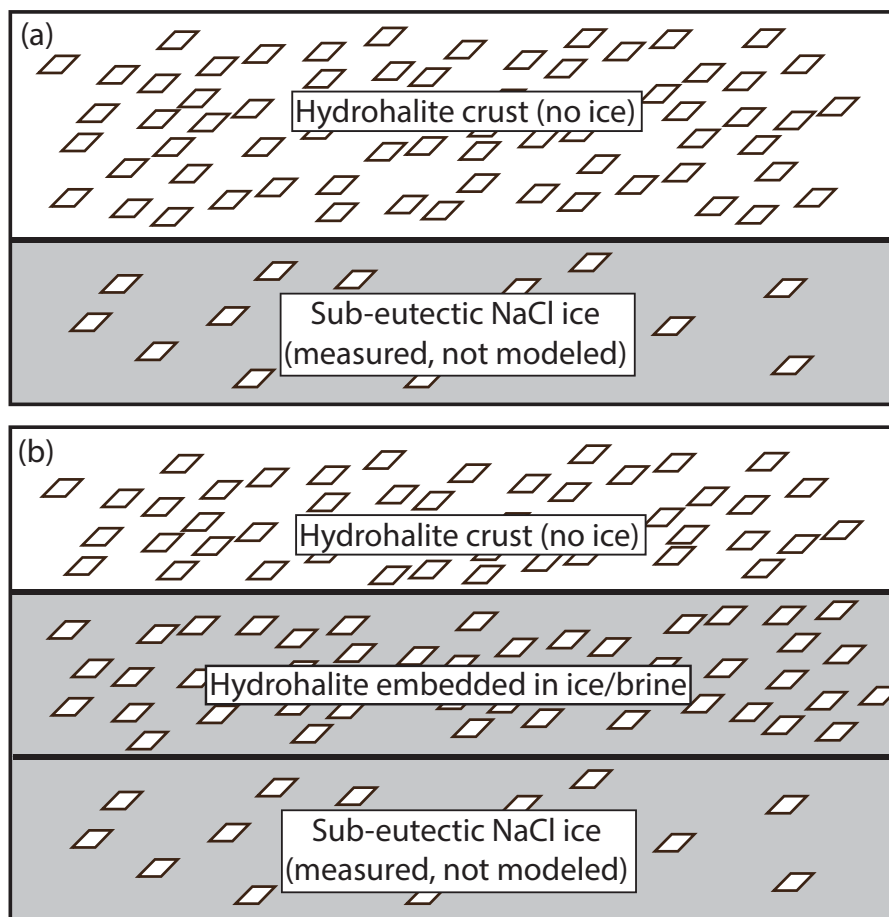


**Figure 2.** Schematic view of layers used to model laboratory measurements. The single-layer model in (a) is used to infer the refractive index of hydrohalite and to parameterize the albedo of hydrohalite crust of different thicknesses. The two-layer model in (b) is used to replicate laboratory measurements. During the development of the crust, the lower layer consists of hydrohalite crystals in an ice medium and represents HH-rich ice; during the dissolution of the crust, the lower layer consists of hydrohalite crystals in a brine medium and represents the partially dissolved crust. In all cases, the albedo of the lowest layer is the measured albedo of subeutectic saline ice.

### 3. Optical Modeling

The laboratory measurements include spectral albedos for (a) subeutectic NaCl ice, (b) ice with the HH-rich ice layer, and (c) the hydrohalite crust of increasing thickness as it gradually replaced the HH-rich layer. These results give some idea of the albedos that can be expected from sea-ice surfaces and hydrohalite crusts, but in order to create an accurate parameterization of hydrohalite crusts on sea ice, we need albedos for a wider range of scenarios. In order to generalize the results to the various surfaces that could exist on Snowball Earth, we used the laboratory measurements to calibrate a radiative transfer model for mixtures of hydrohalite and ice, allowing us to compute spectral and broadband albedos for any combination of crust thickness, individual salt grain size, and salt concentration.

Several configurations were modeled, representing different stages of the laboratory experiment as well as what hydrohalite crust growth might look like in the “natural” setting of Snowball Earth. We first use a simple single-layer model of a hydrohalite crust over a subeutectic sea ice surface to infer the optical properties of hydrohalite, as described in section 3.1. With these properties, we were able to make two-layer models to represent the laboratory scenarios of sublimating HH-rich ice (section 3.2) and dissolving hydrohalite crust (section 3.3). Finally, we returned to a single-layer model to parameterize the albedo of a hydrohalite crust developing through the sublimation of ordinary (non-HH-rich) saline ice. All of these models used the measured albedo of the subeutectic tank surface as their lower boundary. Figure 2 shows schematics.

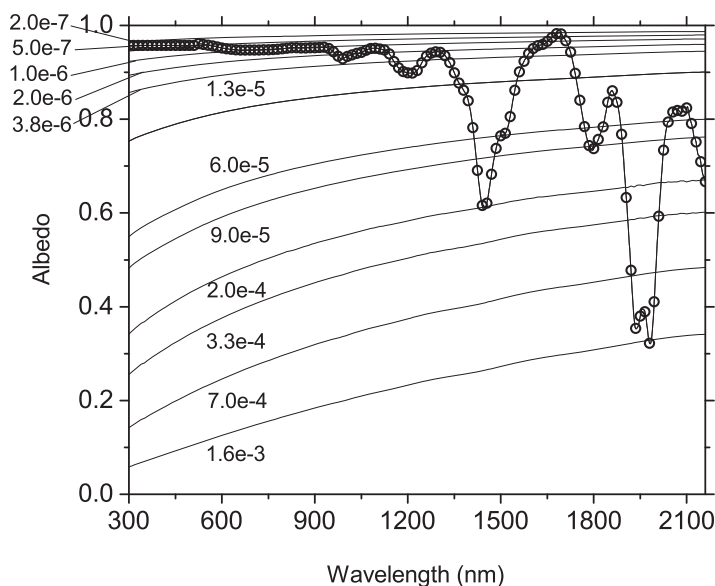


**Figure 3.** The measured albedo of the hydrohalite crust (from *Light et al.* (companion paper), Figure 5) with selected curves superimposed, of albedo calculated using the imaginary refractive index ( $m_{im}$ ) independent of wavelength. The curve of constant  $m_{im}$  that intersects with the albedo measurement at a particular wavelength gives the inferred value of  $m_{im}$  for that wavelength. The curves are labeled with the value of  $m_{im}$ , where (for example) “6.0e-4” means  $6 \times 10^{-4}$ . One hundred and twenty-nine curves were calculated; the few curves shown here were chosen arbitrarily to demonstrate the method.

Well-tested models for Mie scattering [*Wiscombe, 1980*] and discrete-ordinates radiative transfer [*Stamnes et al., 1988*] already exist. The optical properties of pure ice are well known [*Warren and Brandt, 2008*]. Less work exists on the optical properties of hydrohalite. *Wagner et al.* [2012] inferred optical constants for hydrohalite in the infrared from 1.6 to 12.5  $\mu\text{m}$  by spraying a mixture of sodium chloride and water into a chamber at 216 K and measuring the infrared extinction spectra of the resulting aerosol of hydrohalite crystals. For purposes of determining the albedo, however, measurements for visible and near-infrared wavelengths ( $\lambda = 0.3 \mu\text{m}$  to  $\lambda = 2.5 \mu\text{m}$ ) are needed, outside of the wavelength range measured by *Wagner et al.*

### 3.1. Inferring Optical Properties of Hydrohalite

*Light et al.* [2009] estimated the real refractive index of hydrohalite crystals to be  $1.49 \pm 0.02$ . To completely describe the ice-hydrohalite mixture, we also require the imaginary part of the refractive index,  $m_{im}$ , in order to specify the absorption. We lack crystals of sufficient size to measure this property directly, but we can use our measurements of the albedo of the hydrohalite crust as the input to a simple inverse problem. For each wavelength, we can guess a value for  $m_{im}$ , then use this guess as input to the Mie scattering computation, and use the radiative transfer model to compare with the albedo measured in the laboratory. Since we assumed that our highest measured albedo corresponded to the complete replacement of the HH-rich ice layer by hydrohalite crust, we modeled the scenario using a single layer of hydrohalite crystals in air, with the measured albedo of the subeutectic sea ice surface as a lower boundary (see Figure 2a.).

Our measurements below 500 nm were too noisy to use, due to low light levels in the laboratory. To extend our results to more of the visible spectrum, we averaged the albedo values between 495 and 505 nm, then assigned that value to all wavelengths between 300 and 500 nm. In this range, sodium chloride is essentially nonabsorbing, and the absorption coefficients for ice decrease with decreasing wavelength. Thus the overall absorption in this region is likely to be very low, and we feel confident that the albedo in this region would be as high or higher than the albedo at 500 nm if we were able to measure it. Small changes in measured albedo in the 300–600 nm region, where albedos are very high, may lead to large differences in the inferred refractive index. Since the measured albedo is likely to be lower than that of a truly semi-infinite layer of pure hydrohalite, due to its lower thickness and the possible presence of impurities, the inferred index should be viewed as an upper bound.

For each target wavelength (10 nm intervals between 300 and 2200 nm), we ran the model for 129 possible values of the imaginary refractive index, then compared our results to the laboratory measurements and chose the value of  $m_{im}$  that yielded the model-predicted albedo most closely matching the measured albedo. Figure 3 shows the spectral albedo curve measured for the hydrohalite crust and the points where  $m_{im}$  was calculated, along with some example albedo curves using constant  $m_{im}$ . This method was also used by *Skiles* [2014] to infer the imaginary index of dust in snow and *Light et al.* [1998] to infer the imaginary index of sediment in sea ice.

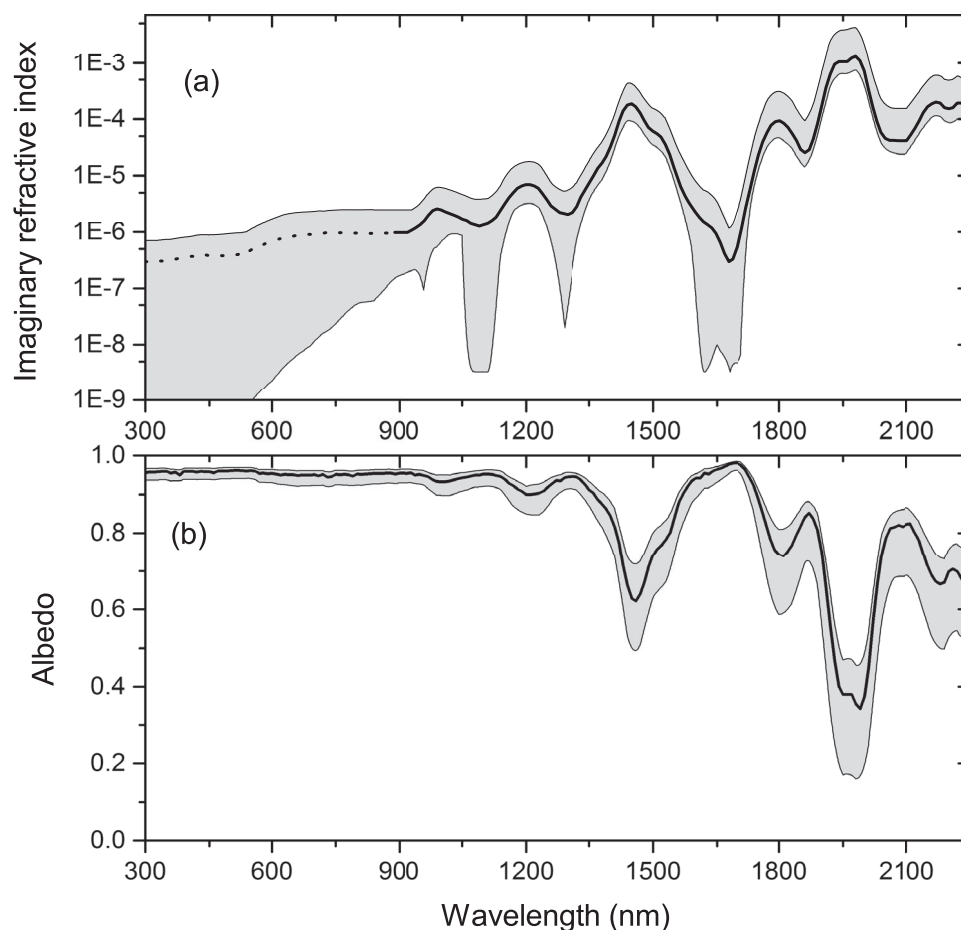


**Figure 4.** Sensitivity of the method to different assumptions about grain size and crust thickness. Assuming large grains (12  $\mu\text{m}$ ) and 2 mm crust gives the lower bound on  $m_{im}$ ; assuming small grains (7  $\mu\text{m}$ ) and semi-infinite crust (10 m) gives an upper bound. Shown are (a) the variation in inferred values of  $m_{im}$  based on different grain size assumptions and (b) the variation in albedo output by the model using identical conditions (semi-infinite crust and 7  $\mu\text{m}$  hydrohalite spheres) but varying the  $m_{im}$  values by the same amount shown in Figure 4a. The imaginary refractive index at wavelengths shorter than 900 nm is represented by a dashed line due to the larger uncertainty in this region. The true value is likely much lower.

Grain size is a key input value for the Mie scattering computation; this estimated grain size was the largest source of uncertainty in this calculation. The hydrohalite grains were irregularly shaped, but we estimated their “equivalent spheres” radius  $r_e$  using the prescription of Grenfell and Warren [1999], in which a non-spherical crystal is represented by a collection of independent spheres having the same total volume and same total surface area as the collection of crystals being simulated. The surface area of a given quantity of material can also be expressed as specific surface area (SSA), which is defined as the surface area per unit mass (with units of  $\text{m}^2 \text{kg}^{-1}$ ). It is reciprocally related to  $r_e$ :  $\text{SSA} = 3/r_e\rho$ , where  $\rho$  is the density of the pure material. We based our initial estimate of  $r_e$  on previous measurements of hydrohalite crystals in brine inclusions of sea ice [Light *et al.*, 2009]. This initial estimate provided only an upper bound to the effective radius of the crystals. Light *et al.* [2009] found the crystals to be highly irregular in shape; Dang *et al.* (manuscript submitted to *J. Atmos. Sci.*, 2016) found that, in snow, the albedo produced by non-spherical grains could be matched by spherical grains of smaller size.

Our estimate was also influenced by the results of our modeling; larger grain sizes could not reproduce the observed albedos without using physically implausible crust thicknesses. The thickest measured laboratory crust was optically thick at most wavelengths, but may not have been so at the wavelengths where hydrohalite is most transparent (especially in the visible between 300 and 800 nm, and at the peak near 1700 nm). The estimated crust thickness added some uncertainty to our results at these wavelengths. Figure 4a shows the possible error in our inference of  $m_{im}$  based on varying the modeled particle radius between 3 and 12  $\mu\text{m}$ , centered at 7  $\mu\text{m}$ , and based on varying the estimated crust thickness between

2mm and optically semi-infinite (we arbitrarily chose 10 m as the optically semi-infinite depth.) Figure 4b shows the error in albedo associated with the different values of  $m_{im}$ . Note that, while the error in estimated  $m_{im}$  is relatively large at the wavelengths where hydrohalite is most transparent, this uncertainty leads to relatively little uncertainty in the albedo, since it is already close to 1.0 at those wavelengths.

### 3.2. Sublimating Hydrohalite-Enriched Ice

Using these results for the optical properties of hydrohalite, we modeled the initial laboratory scenario of an ice-hydrohalite mixture and followed its progression as an ice-free hydrohalite crust formed over the mixed layer and grew thicker. Figure 2b shows a schematic view of this model. The model treats the ice-hydrohalite mixture as an ice medium containing grains of hydrohalite, rather than using air as a medium for a mixture of ice and hydrohalite grains. We used the methods outlined in *Mullen and Warren* [1988] for dealing with a scatterer in an absorbing medium. The methods were originally developed using nonabsorbing bubbles in lake ice as the scatterer, so we made modifications to account for the fact that hydrohalite does absorb some light, as follows.

The effective complex refractive index of the hydrohalite embedded within the ice is given by  $m_{hh}/m_i$ , where  $m_{hh}$  is the complex refractive index of hydrohalite and  $m_i$  is the complex refractive index of ice. Using this effective index as input to the Mie scattering computation gives the asymmetry factor and the scattering efficiency of the ice/hydrohalite mixture. Following *Mullen and Warren* [1988], the absorption coefficient is approximated simply as

$$\kappa_{mix} = f_{ice}\kappa_{ice} + f_{hh}\kappa_{hh}, \quad (1)$$

where  $f_{ice}$  and  $f_{hh}$  are the volume fractions of ice and hydrohalite and  $\kappa_{ice}$  and  $\kappa_{hh}$  are the absorption coefficients.

The single-scattering coalbedo is related to the scattering efficiency as

$$(1 - \tilde{\omega}) = \frac{\kappa_{mix}}{\kappa_{mix} + \sigma_{mix}} \quad (2)$$

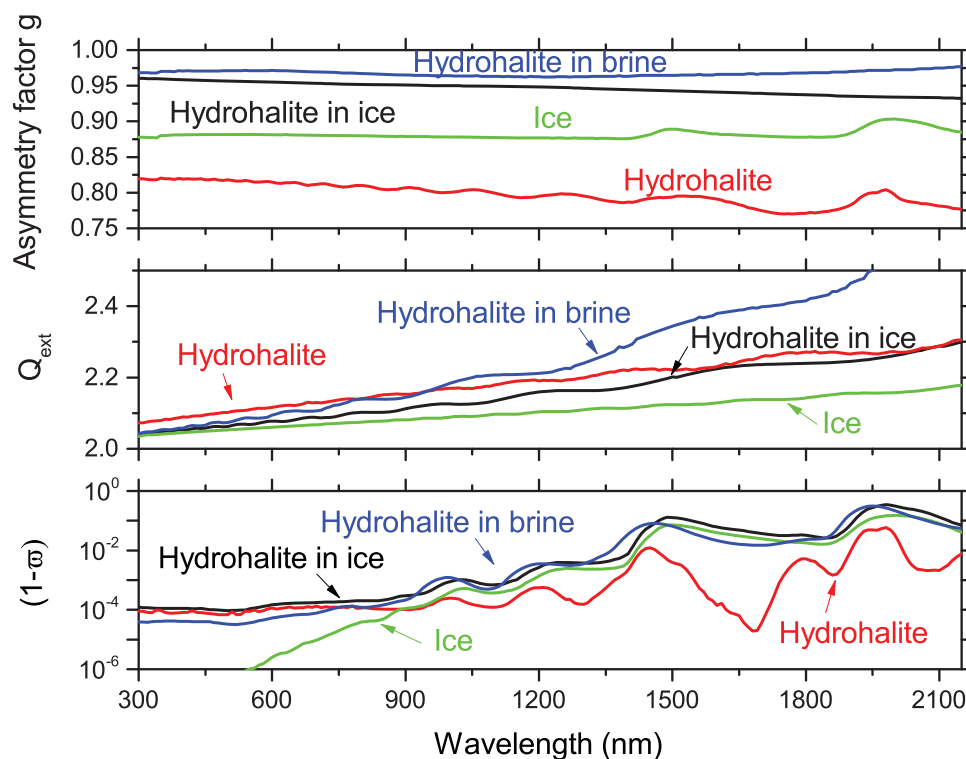


**Figure 5.** Asymmetry factor  $g$ , extinction efficiency  $Q_{ext}$  and single-scattering coalbedo  $(1 - \tilde{\omega})$  and single-scattering coalbedo for hydrohalite spheres in air, and hydrohalite spheres embedded in ice. For purposes of comparison, the size of the spheres in all cases is  $7 \mu\text{m}$ .

where the scattering coefficient  $\sigma$  is given by

$$\sigma = Q_{sca} \pi r^2 N \tag{3}$$

Here  $Q_{sca}$  is the scattering efficiency,  $r$  is the effective radius of the particles, and  $N$  is the number density of the particles. In this case, we assume the particles to be monodisperse for simplicity. The asymmetry factor ( $g$ ) is useful for representing the single-scattering phase function; it is the average cosine of the scattering angle. It is a standard output from Mie theory and varies between  $-1$  (complete backscatter) and  $+1$  (exclusively forward scattering). Figure 5 shows the inherent optical properties of ice spheres in air, hydrohalite spheres in air, hydrohalite spheres embedded in ice, and hydrohalite spheres embedded in brine.

The model starts with a single layer of HH-rich ice. At the next step, the model adds a layer of hydrohalite crust; each subsequent step of the sublimation progressively increases the thickness of the hydrohalite crust layer, reducing the thickness of the HH-rich ice layer by a prescribed amount and adding the same thickness to the hydrohalite crust. Finally the HH-rich ice layer is completely replaced by hydrohalite crust, representing the complete sublimation of the ice matrix. The effective radius used for the hydrohalite crystals embedded within the ice is  $20 \mu\text{m}$ . Note that this is larger than the effective radius used for the hydrohalite crust ( $7 \mu\text{m}$ ), as the larger radius was necessary to match the shape of the measured laboratory albedos. This may be due to a change in the geometry of the hydrohalite crystals during the sublimation process; alternatively, the grain radius may be acting as a proxy for another process that was not included in the model. The model does not attempt to represent processes such as sublimation over time. The modeled crust thicknesses are chosen to match the measured albedo results.

Figure 6 shows measured laboratory albedos plotted along with modeled albedos of HH-rich ice with a hydrohalite crust. The 42 day laboratory albedo was used as a target in determining the optical properties of hydrohalite, so we would expect the modeled crust albedo to match it. In practice, there are slight

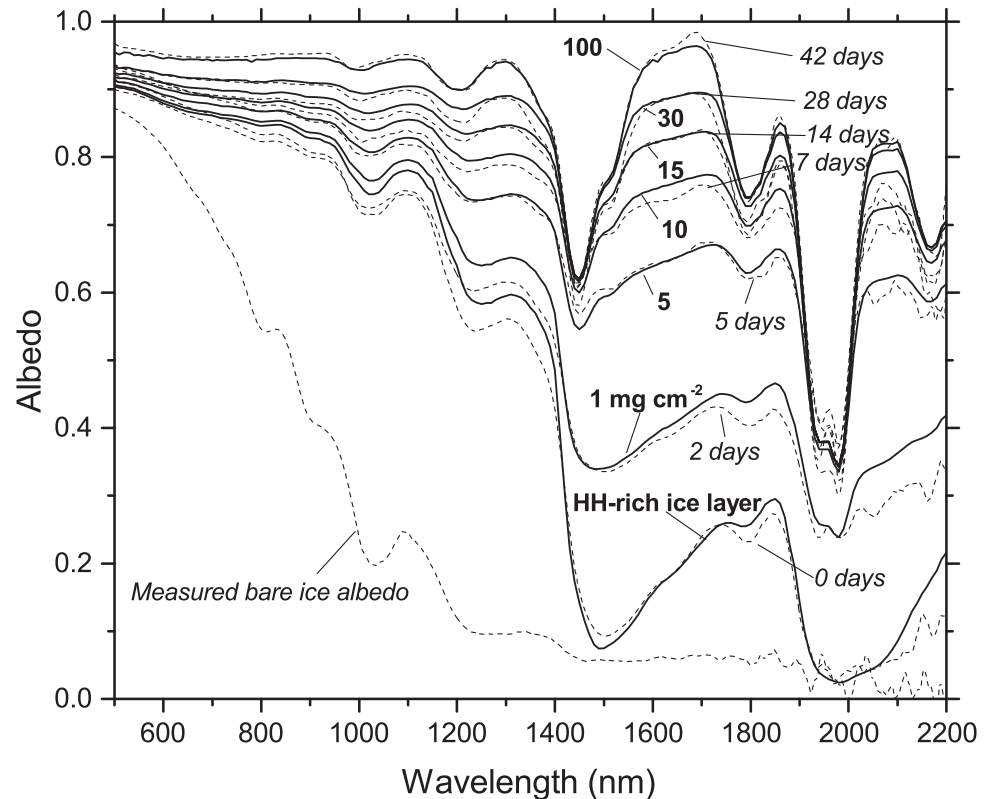


**Figure 6.** Comparison of modeled and measured spectral albedos for different thicknesses of hydrohalite-rich ice layer and hydrohalite crust. Dashed lines (labeled with italic text) show albedos measured in the laboratory; solid lines show albedo output from the model (for diffuse incidence, since the light in the dome is diffuse.) Hydrohalite crust thickness for the model output is labeled in milligrams per square centimeter.

differences due to smoothing of the hydrohalite optical properties. The modeled HH-rich ice layer, without a hydrohalite crust layer on top of it, matches the laboratory HH-rich ice layer closely in infrared wavelengths, but appears to be too high at visible wavelengths.

### 3.3. Dissolving Hydrohalite Crust

Laboratory measurements were also made of a warming hydrohalite crust as it dissolved. This situation is expected to be transient, since any sodium chloride brine supersaturated enough to preserve hydrohalite crystals would melt the ice underneath it until it reached equilibrium. However, the strong positive feedback produced by the dissolution means that melting crust albedos could be important for simulating climatic response to specific events where a change in phase causes a sharp transition in albedo. We attempted to model the dissolving crust using the same methods as for the HH-rich ice, with hydrohalite crystals embedded in brine (Figure 7.) Refractive indices used for the brine may be found in *Maykut and Light* [1995]. The model shows a progression as a lower layer of hydrohalite-rich brine gradually increases in thickness, replacing the layer of pure hydrohalite above it. This model does not match the measurements as well as the model of crust development, especially in the near-infrared. This may be due to a mismatch between the modeled scenario and the reality of laboratory conditions. In the model, the layer of dry hydrohalite crust and the layer of hydrohalite-rich brine have a clear boundary, the fraction of hydrohalite in the brine does not change, and the layers are underlain by subeutectic sea ice. In the laboratory, brine may have wicked up through the hydrohalite layer, the fraction of hydrohalite within the brine was probably not constant, and the hydrohalite within the underlying ice would have dissolved at some point during the crust demise. While the details of this process are subject to certain assumptions about the laboratory observations, there is clear evidence that the rapid demise of a hydrohalite crust resulting from warming above  $T_{eu}$  leads to dramatically reduced spectral albedo at all wavelengths.

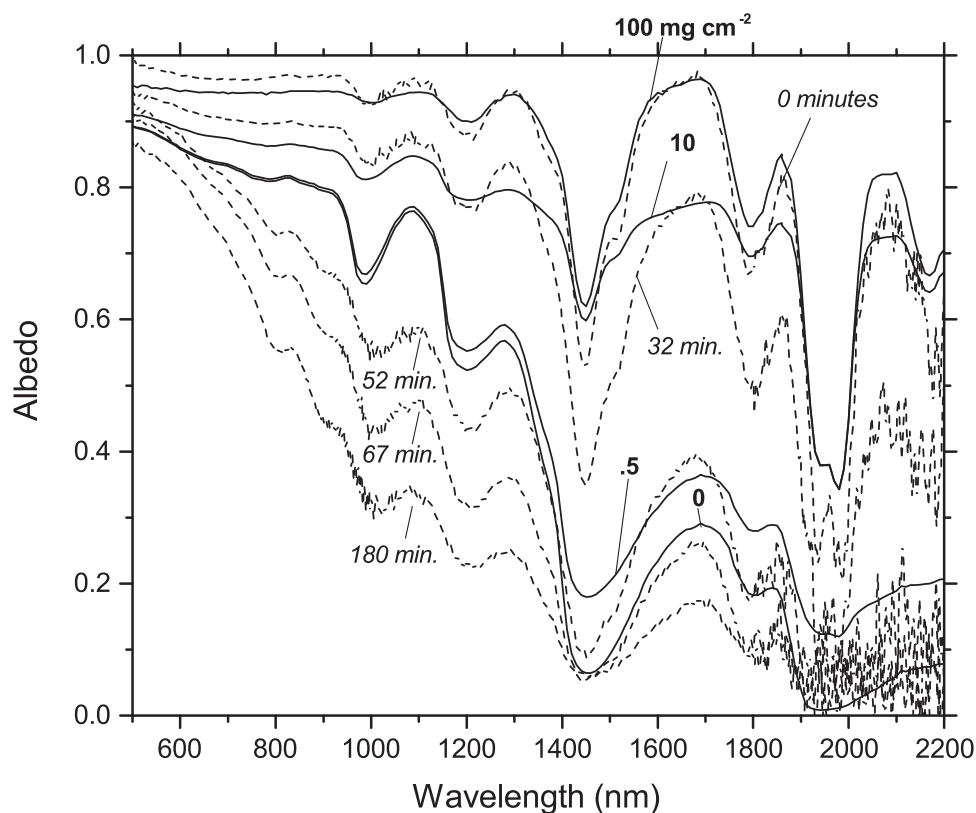


**Figure 7.** Comparison of modeled and measured spectral albedos for a dissolving hydrohalite crust. Due to the delicate and transient nature of the rapidly dissolving hydrohalite crust, we were unable to make any measurements that would tell us what fraction of the hydrohalite remained at any given time step, nor could we know for certain what changes might be occurring in the ice below the hydrohalite layer. Thus the modeled albedos here represent only a rough estimate.

#### 4. Parameterization

This model allows the determination of the albedo of a hydrohalite crust of arbitrary thickness, but is too complex and computationally expensive to include as part of a global climate model (GCM). The model results shown in Figure 6 are also not directly applicable to the case of ordinary sea ice sublimating without melt, since the laboratory crust developed from a layer of ice containing 25% hydrohalite by volume, whereas ordinary first-year sea ice generally contains only ~10‰ of salt. (before significant flushing that typically occurs during summer melt.) In order to represent the natural development of a hydrohalite crust on sea ice, we model a crust of hydrohalite crystals in air over a substrate of subeutectic ice with something closer to normal sea ice salinity. The underlying sea-ice albedo used in this modeling is the albedo measured in the laboratory for subeutectic ice at  $-30^{\circ}\text{C}$ .

We calculated the spectral albedo  $\alpha(\lambda)$  for several crust thicknesses, expressed in units of grams per square centimeter. We integrated these albedos across wavelength bands commonly used in GCMs, weighting the integration using solar spectra  $F(\lambda)$  for polar atmospheres from an atmospheric radiation model [Wiscombe *et al.*, 1984]. Two solar spectra are used, one for clear sky and one for cloudy sky; they are similar to the solar spectra shown in Figure 1 of Brandt and Warren [1993], but adjusted for sea level as described in Figure 6 of Carns *et al.* [2015]. The broadband albedo is then

$$\bar{\alpha} = \frac{\int \alpha(\lambda)F(\lambda)d\lambda}{\int F(\lambda)d\lambda} \tag{4}$$

In this case, we use 300–700 nm as the visible wavelength band, 700–2500 nm as the near-IR wavelength band, and 300–2500 nm for the “allwave” albedo. Figure 8 shows the results of this modeling.

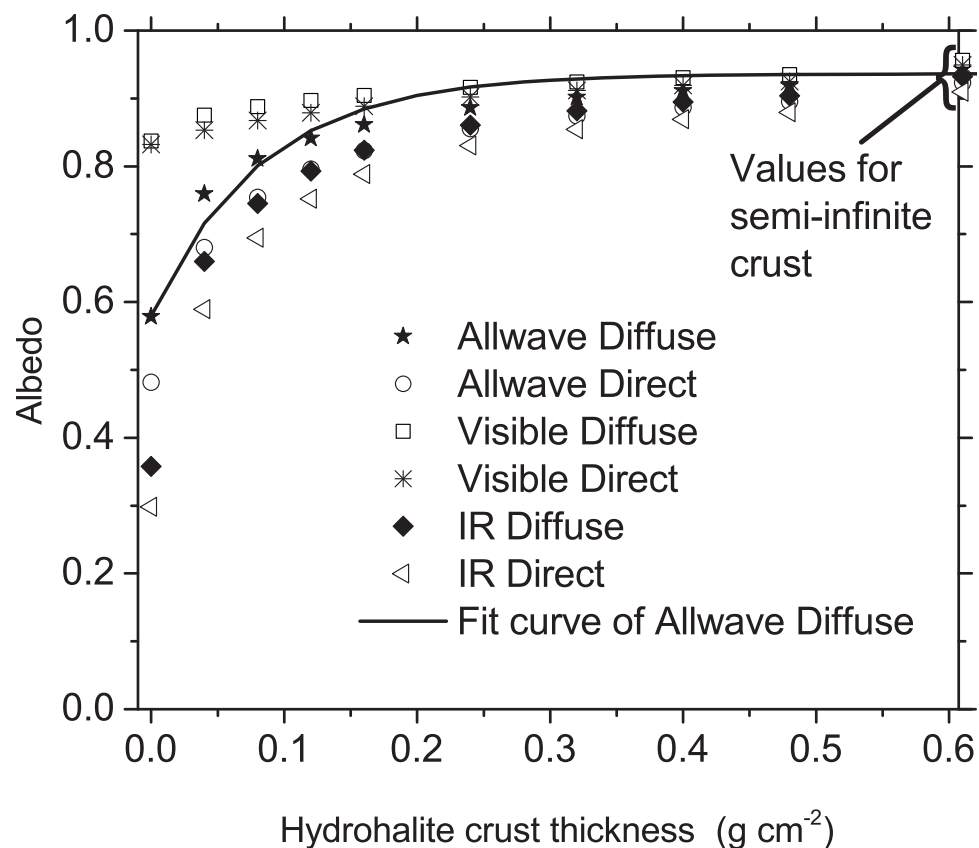


**Figure 8.** Calculations used for parameterization. To avoid cluttering the graph, only one line of fit is shown, the parameterization for diffuse broadband. The fit is forced to be accurate in the limits of zero thickness and semi-infinite thickness; the albedo given by the equation at moderate crust thicknesses is too high.

**Table 1.** Constants for Equation (5)

Band	$y_0$	A	$t$ (g cm <sup>-2</sup> )
Allwave diffuse	0.94	-0.36	0.083
Allwave direct	0.92	-0.43	0.089
Visible diffuse	0.96	-0.12	0.20
Visible direct	0.95	-0.12	0.26
IR diffuse	0.92	-0.56	0.070
IR direct	0.90	-0.60	0.078

Decaying exponential curves (see equation (5)) are fitted to the data points. We used data analysis software (Origin v. 9.1) to fit the data. The data points at zero thickness and optically semi-infinite thickness are weighted 10 times more heavily. This was done to ensure that the parameterization gives accurate results for small thicknesses (where small differences in thickness can make a large difference in albedo) and for the semi-infinite case (toward which all crusts

will tend over time), at the expense of some accuracy at moderate thicknesses. The parameterization is then

$$y = y_0 + Ae^{-x/t}, \tag{5}$$

where  $y$  is the albedo,  $y_0$  is the semi-infinite albedo,  $x$  is the crust thickness in g cm<sup>-2</sup>, and  $t$  is a characteristic (e-folding) thickness. Table 1 gives the constants for equation (5) for clear and cloudy skies in the visible, near-IR and allwave.

In the full sea-salt system, temperatures below the precipitation point of hydrohalite but above the eutectic of seawater (between -23°C and -37°C, if following the precipitation pathway described in Marion *et al.* [1999]) might result in a surface composed of hydrohalite crystals wetted by a brine containing other dissolved salts (such as magnesium chloride.) The composition of the ocean during Snowball Earth is not well constrained, but investigating the effects of other salts on the formation of lag deposits could provide a fruitful avenue for future work.

### 5. Contrasts With Other Surface Albedos on Snowball Earth

The contrast between the albedo of the bright hydrohalite crust and the albedos of other sea-ice surfaces has the potential to introduce new feedbacks into models of Snowball Earth. Without hydrohalite, the primary influence on surface albedo is the freezing or melting of sea ice, at a temperature threshold around -2°C, which is the source of the positive feedback which likely helped promote Snowball Earth events. The next most important is the presence or absence of snow; this is controlled by precipitation and sublimation, which in turn depend on climate and weather patterns.

Adding the effects of precipitated salts introduces new processes. The first is the precipitation of hydrohalite within brine pockets, at a temperature threshold around -23°C (depending on salt composition), which can introduce a small positive feedback as low temperatures increase albedo. The second is the formation

**Table 2.** Albedos for Snowball Earth Surfaces

Ice Type	Albedo (Allwave, Diffuse)	Properties and Processes
Glacier ice (sublimating sea-glacier)	0.5–0.65	Forms from compressed snow. Albedo determined by specific surface area (SSA) and absorbing contaminants (dust, tephra, etc.) [Dadic <i>et al.</i> , 2013]
Firn	0.65–0.8	Forms from compressed snow. Albedo determined by SSA and absorbing contaminants. [Dadic <i>et al.</i> , 2013]
Snow	0.8–0.9	Falls as precipitation. Albedo determined by SSA and absorbing contaminants. [Zatko and Warren, 2015]
Bare sea ice	0.45–0.55	Freezes from seawater. Albedo determined by ice thickness and amount of hydrohalite precipitation, which is determined primarily by temperature. [Carns <i>et al.</i> , 2015]
Hydrohalite crust	0.6–0.9	Exposed by sublimating sea ice. Albedo determined by SSA, absorbing contaminants, and thickness, which is a function of time spent sublimating without melt. (this work)
Dissolving hydrohalite crust	0.3–0.6	Hydrohalite dissolves at around -23°C when in contact with ice. [This work]
Melt ponds	0.1–0.5	May form at 0° in the absence of a hydrohalite crust; with crust, forms at -23°C. [Perovich <i>et al.</i> , 2002]

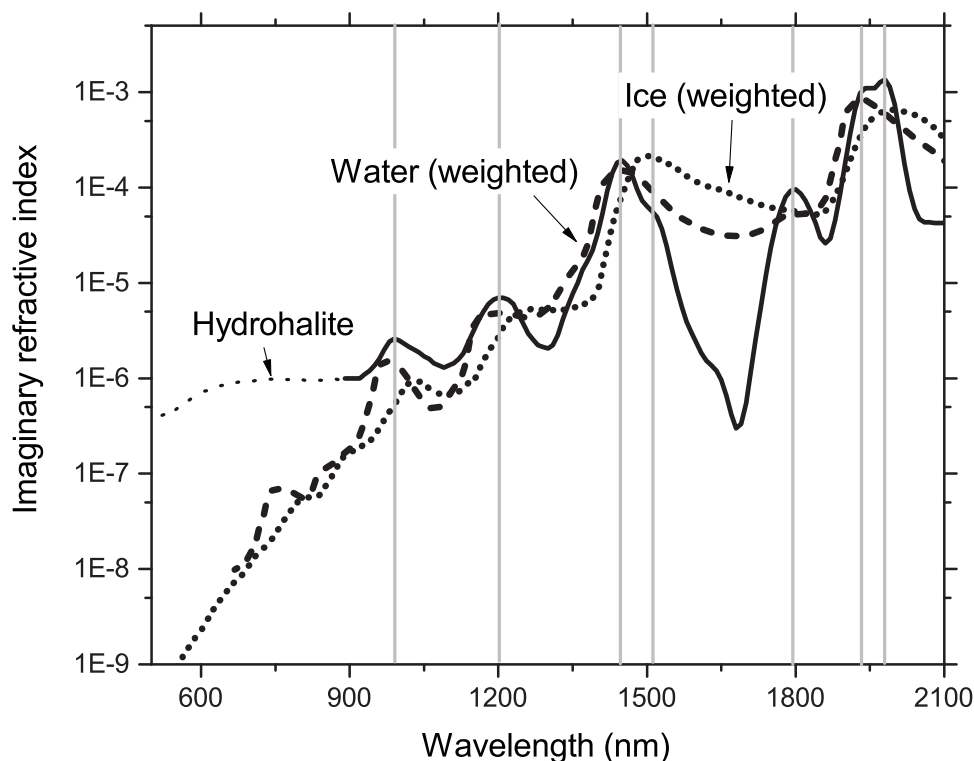


**Figure 9.** Comparison of imaginary refractive indices of water [Kou *et al.*, 1993], ice [Warren and Brandt, 2008], and hydrohalite. Water and ice indices are weighted to reflect the mass fraction of water molecules in hydrohalite compared to the mass fraction of sodium and chloride atoms (which do not contribute to absorption in this wavelength range and are assumed to have an effective imaginary refractive index of 0.) Vertical lines show some of the hydrohalite absorption peaks. Hydrohalite is represented by a dashed line at wavelengths below 900 nm to indicate that measurements here are relatively more uncertain than measurements in other wavelength ranges, and the true value of the imaginary refractive index is likely much closer to that of water and ice.

of a hydrohalite crust by sublimation of the surrounding ice; like the sublimation of snow, this depends on climate to maintain negative values for precipitation minus evaporation (P-E). The third is the dissolution of the hydrohalite crust, which again occurs around  $-23^{\circ}\text{C}$ , and introduces a potentially potent positive feedback between increasing temperatures and decreasing albedo. Table 2 places hydrohalite crust albedo in context with albedos of other Snowball Earth surfaces.

A similar result was found for  $\text{CaSO}_4$ . Comparing the spectrum of the anhydrous mineral to the spectra of two hydrated forms ( $\text{CaSO}_4 \cdot 0.5\text{H}_2\text{O}$ , bassanite and  $\text{CaSO}_4 \cdot 2\text{H}_2\text{O}$ , gypsum), Bishop *et al.*, [2014] assigned the absorption features of the hydrated minerals in the region  $1.3\text{--}2.5\ \mu\text{m}$  to combinations and overtones of the fundamental vibration bands of  $\text{H}_2\text{O}$ . For water vapor, the fundamental bands are located at  $2.66\ \mu\text{m}$  (asymmetric stretch),  $2.73\ \mu\text{m}$  (symmetric stretch), and  $6.27\ \mu\text{m}$  (bending) [Eisenberg and Kauzmann, 1969, Table 1.3]. The overtones and combinations occur at higher frequency (smaller wavelength), and their locations in ice are shifted slightly from their locations in liquid water. The fact that hydrohalite displays absorption features of both water and ice (Figure 9) suggests that one of the two waters of hydration might be in an electrostatic environment similar to that in liquid water, with the other water molecule in an ice-like environment. The crystal structure of hydrohalite [Klewe and Pedersen, 1974] does show the two water molecules to be in slightly different environments, but it is by no means apparent that one is more liquid-like and other more ice-like.

## 6. Discussion

In addition to its relevance to the energy balance of Snowball Earth, the modeling described here also provides a determination of the imaginary refractive index of hydrohalite in the visible region. Figure 9 compares this imaginary refractive index to those of ice and water. Sodium chloride is nonabsorbing in the wavelength range measured, so we expect all absorption to be due to the water molecules in the hydrated

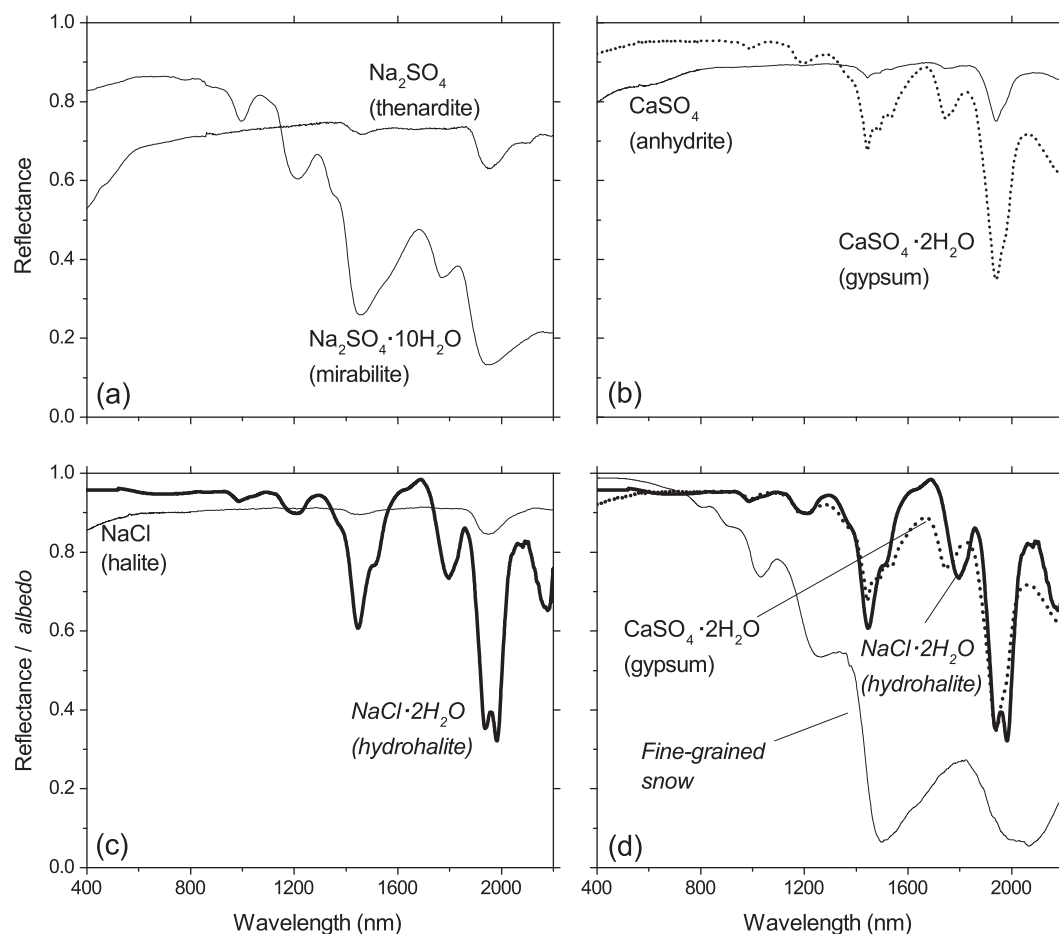


**Figure 10.** Comparison of reflectances and albedos of different hydrated and anhydrous minerals. Shown are (a) mirabilite, another hydrated mineral that precipitates in brine inclusions in sea ice, compared to its anhydrous form thenardite; (b) gypsum, a dihydrate mineral like hydrohalite, compared to its anhydrous form anhydrite; (c) hydrohalite compared to its anhydrous form halite; and (d) hydrohalite compared to gypsum, demonstrating the similarity in their spectral reflectance, with snow albedo for comparison. Mineral reflectances, except for hydrohalite, are laboratory measurements from the ASTER spectral library [Baldrige *et al.*, 2009]; snow albedo is from Hudson *et al.* [2006]. Note that for salts such as NaCl, which is essentially nonabsorbing in this wavelength range, the ASTER “reflectance” is lower than the albedo of a halite surface would be.

crystal. Note the doublet around 1950 nm, where the absorption peaks of water and ice are relatively far apart, and the shoulder peak around 1500 nm, which appears to line up with an absorption peak of ice. The absorption bands of hydrohalite appear to be narrower than those of water or ice, resulting in less overlap between peaks.

It is interesting to compare the albedo measurements of sodium chloride dihydrate to reflectance measurements of nonhydrated sodium chloride, as well as to other hydrated salts (Figure 10). The reflectance measurements for salts cited here come from the ASTER spectral database [Baldrige *et al.*, 2009]. Figure 10d shows a comparison of the albedo measurements used in this study with reflectance measurements of gypsum, another dihydrate mineral. Both show absorption bands around 1400 and 2000 nm, where water absorbs very strongly; note that even the anhydrous forms of the minerals (Figures 10b and 10c) show small amounts of absorption at the same locations, presumably due to small quantities of water adsorbed onto their surface from the atmosphere. Figure 10a shows the reflectance spectrum of mirabilite, another hydrated salt known to precipitate in sea ice, and its anhydrous form thenardite. Mirabilite, with formula  $\text{Na}_2\text{SO}_4 \cdot 10\text{H}_2\text{O}$ , shows much stronger absorption in the infrared than gypsum or hydrohalite.

Our laboratory measurements show that the albedo of a hydrohalite lag deposit is as high as that of fresh snow at visible wavelengths, and higher in the near-IR where snow is more absorptive, indicating that such hydrohalite crusts could strongly alter the surface energy balance of Snowball Earth. The simplified

laboratory scenario studied here included only water and sodium chloride; the full complement of salts in ocean water would likely change the results. Sodium chloride would still precipitate, and possibly at a similar temperature; in brine inclusions within modern sea ice it begins to precipitate around  $-23^{\circ}\text{C}$ . However, other salts such as potassium chloride or magnesium chloride could depress the freezing point of the remaining brine below this temperature. Laboratory experiments have also shown that sodium chloride solutions can supercool below their eutectic point. Carns *et al.* [2015] found that brine inclusions in sea ice can supercool by as much as 6 K below the precipitation point of hydrohalite; Toner *et al.* [2014] found supercooling of up to 8.3 K in solutions of pure sodium chloride.

Depending on the freezing pathway, modern seawater may reach its eutectic point at about  $-37^{\circ}\text{C}$ , when magnesium chloride dodecahydrate ( $\text{MgCl}_2 \cdot 12\text{H}_2\text{O}$ ) precipitates [Marion *et al.*, 1999]. Below this eutectic point, with all salts precipitated, the sea ice might develop a salt crust similar to that investigated in this study. Between  $-23^{\circ}\text{C}$  and the eutectic, the presence of these other salts would result in a slush of hydrohalite crystals and concentrated brine. Measuring the albedo of such a surface, and investigating the effects of a prolonged period of desiccation, could provide a subject for future work.

## 7. Conclusions

Precipitated salt within sea ice can alter the ice albedo at low temperatures. The albedo increases slightly when salt precipitates within brine pockets, and more dramatically when ice sublimates away and the salt is left as a cryogenite lag deposit. This can lead to two different positive feedbacks. The first is the precipitation feedback: salt precipitation occurs when temperature decreases below  $-23^{\circ}\text{C}$ , increasing albedo slightly, which would cause temperature to drop further (if supercooling occurs, the threshold may be somewhat lower, as described by Carns *et al.* [2015]). Conversely, temperatures increasing above this threshold would cause precipitated hydrohalite to dissolve, decreasing albedo and causing temperatures to rise further. The second feedback is the crust-dissolution feedback: once a lag deposit of hydrohalite develops, it will begin to dissolve at a temperature of  $-23^{\circ}\text{C}$ , potentially decreasing the albedo from above 0.9 to below 0.4. (The development of the crust probably does not qualify as a positive feedback, since it will occur only after an extended period of low temperatures and net sublimation.)

The results in this paper may also be of some interest to the planetary science community in performing spectral analyses of substances found on the surface of icy moons. For instance, Europa is likely to be relatively rich in Na and Cl ions, which could form hydrohalite on its surface [Carlson *et al.*, 2009; Brown and Hand, 2013].

## Acknowledgments

The data for this paper are available at <http://dx.doi.org/10.6084/m9.figshare.1267444>. This work was supported by NSF grants ANT-0739779 and ANT-1142963. A Postdoctoral Fellowship from the UW Future of Ice Initiative to TC is gratefully acknowledged.

## References

- Adams, L. H., and R. E. Gibson (1930), The melting curve of sodium chloride dihydrate. An experimental study of an incongruent melting at pressures up to twelve thousand atmospheres, *J. Am. Chem. Soc.*, *52*(1905), 4252–4264, doi:10.1021/ja01374a010.
- Baldrige, A. M., S. J. Hook, C. I. Grove, and G. Rivera (2009), The ASTER spectral library version 2.0, *Remote Sens. Environ.*, *113*(4), 711–715, doi:10.1016/j.rse.2008.11.007.
- Bishop, J. L., M. D. Lane, M. D. Dyar, S. J. King, A. J. Brown, and G. Swayze (2014), Spectral properties of Ca-sulfates: Gypsum, bassanite, and anhydrite, *Am. Mineral.*, *99*(10), 2105–2115.
- Brandt, R. E., and S. G. Warren (1993), Solar-heating rates and temperature profiles in Antarctic snow and ice, *J. Glaciol.*, *39*(131), 99–110.
- Brandt, R. E., S. G. Warren, A. P. Worby, and T. C. Grenfell (2005), Surface albedo of the Antarctic sea ice zone, *J. Clim.*, *18*(17), 3606–3622, doi:10.1175/JCLI3489.1.
- Brown, M. E., and K. P. Hand (2013), Salts and radiation products on the surface of Europa, *Astron. J.*, *145*(4), article no. 110.
- Budyko, M. I. (1969), The effect of solar radiation variations on the climate of the Earth, *Tellus*, *21*(5), 611–619, doi:10.3402/tellusa.v21i5.10109.
- Carlson, R., W. Calvin, and J. Dalton (2009), Europa's surface composition, in *Europa*, pp. 283–327, Univ. of Ariz. Press, Tucson.
- Carns, R. C., R. E. Brandt, and S. G. Warren (2015), Salt precipitation in sea ice and its effect on albedo, with application to Snowball Earth, *J. Geophys. Res. Oceans*, *120*, 2370–2384, doi:10.1002/2014JC010516.
- Carns, R. C., Light, B., and S. G. Warren (2016), The spectral albedo of sea ice and salt crusts on the tropical ocean of Snowball Earth: II. Optical modeling, *J. Geophys. Res. Oceans*, doi:10.1002/2016JC011804, in press.
- Dadic, R., P. C. Mullen, M. Schneebeli, R. E. Brandt, and S. G. Warren (2013), Effects of bubbles, cracks, and volcanic tephra on the spectral albedo of bare ice near the Transantarctic Mountains: Implications for sea glaciers on Snowball Earth, *J. Geophys. Res. Earth Surf.*, *118*, 1658–1676, doi:10.1002/jgrf.20098.
- Dang, C., Q. Fu, and S. G. Warren (2016), Effect of snow grain shape on snow albedo, *J. Atmos. Sci.*, doi:10.1175/JAS-D-15-0276.1, in press.
- Dieckmann, G. S., G. Nehrke, S. Papadimitriou, J. Göttlicher, R. Steininger, H. Kennedy, D. Wolf-Gladrow, and D. N. Thomas (2008), Calcium carbonate as ikaite crystals in Antarctic sea ice, *Geophys. Res. Lett.*, *35*, L08501, doi:10.1029/2008GL033540.
- Dieckmann, G. S., G. Nehrke, C. Uhlig, J. Göttlicher, S. Gerland, M. A. Granskog, and D. N. Thomas (2010), Brief Communication: Ikaite ( $\text{CaCO}_3 \cdot 6\text{H}_2\text{O}$ ) discovered in Arctic sea ice, *Cryosphere*, *4*, 227–230, doi:10.5194/tc-4-227-2010.

- Eisenberg, D., and W. Kauzmann (1969), *The Structure and Properties of Water*, Clarendon Press, Oxford.
- Golden, K. M., S. F. Ackley, and V. I. Lytle (1998), The percolation phase transition in sea ice, *Science*, 282(5397), 2238–2241, doi:10.1126/science.282.5397.2238.
- Grenfell, T. C., and S. G. Warren (1999), Representation of a nonspherical ice particle by a collection of independent spheres for scattering and absorption of radiation, *J. Geophys. Res.*, 104(D24), 31,697–31,709.
- Hoffman, P. F., and D. P. Schrag (2002), The snowball Earth hypothesis: Testing the limits of global change, *Terra Nov.*, 14(3), 129–155, doi:10.1046/j.1365-3121.2002.00408.x.
- Hu, Y.-B., D. A. Wolf-Gladrow, G. S. Dieckmann, C. Völker, and G. Nehrke (2014), A laboratory study of ikaite (CaCO<sub>3</sub>·6H<sub>2</sub>O) precipitation as a function of pH, salinity, temperature and phosphate concentration, *Mar. Chem.*, 162, 10–18, doi:10.1016/j.marchem.2014.02.003.
- Hudson, S. R., S. G. Warren, R. E. Brandt, T. C. Grenfell, and D. Six (2006), Spectral bidirectional reflectance of Antarctic snow: Measurements and parameterization, *J. Geophys. Res.*, 111, D18106, doi:10.1029/2006JD007290.
- Kirschvink, J. L. (1992), Late Proterozoic low-latitude global glaciation: The snowball Earth, in *The Proterozoic Biosphere*, vol. 52, edited by J. W. Schopf and C. Klein, pp. 51–52, Cambridge Univ. Press, Cambridge.
- Klewe, B., and B. Pedersen (1974), The crystal structure of sodium chloride dihydrate, *Acta Crystallogr.*, B30(3), 2363–2371, doi:10.1107/S0567740874007138.
- Kou, L., D. Labrie, and P. Chylek (1993), Refractive indices of water and ice in the 0.65- to 2.5- $\mu$ m spectral range, *Appl. Opt.*, 32(19), 3531–3540, doi:10.1364/AO.32.003531.
- Light, B., H. Eicken, G. A. Maykut, and T. C. Grenfell (1998), The effect of included particulates on the spectral albedo of sea ice, *J. Geophys. Res.*, 103(C12), 27739–27752, doi:10.1029/98JC02587.
- Light, B., G. A. Maykut, and T. C. Grenfell (2003), Effects of temperature on the microstructure of first-year Arctic sea ice, *J. Geophys. Res.*, 108(C2), 3061, doi:10.1029/2001JC000887.
- Light, B., R. E. Brandt, and S. G. Warren (2009), Hydrohalite in cold sea ice: Laboratory observations of single crystals, surface accumulations, and migration rates under a temperature gradient, with application to “Snowball Earth,” *J. Geophys. Res.*, 114, C07018, doi:10.1029/2008JC005211.
- Light, B., R. C. Carns, and S. G. Warren (2015), “Albedo dome”: A method for measuring spectral flux-reflectance in a laboratory for media with long optical paths, *Appl. Opt.*, 54(17), 5260–5269, doi:10.1364/AO.54.005260.
- Light, B., R. C. Carns, and S. G. Warren (2016), The spectral albedo of sea ice and salt crusts on the tropical ocean of Snowball Earth: I. Laboratory measurements, *J. Geophys. Res. Oceans*, doi:10.1002/2016JC011803, in press.
- Marion, G. M., R. E. Farren, and A. J. Komrowski (1999), Alternative pathways for seawater freezing, *Cold Reg. Sci. Technol.*, 29(3), 259–266, doi:10.1016/S0165-232X(99)00033-6.
- Maykut, G. A., and B. Light (1995), Refractive-index measurements in freezing sea-ice and sodium chloride brines, *Appl. Opt.*, 34(6), 950–961.
- Mullen, P. C., and S. G. Warren (1988), Theory of the optical properties of lake ice, *J. Geophys. Res.*, 93(7), 8403–8414.
- Payne, R. E. (1972), Albedo of the sea surface, *J. Atmos. Sci.*, 29(5), 959–970, doi:10.1175/1520-0469(1972)029<0959:AOTSS>2.0.CO;2.
- Pegau, W. S., and C. A. Paulson (2001), The albedo of Arctic leads in summer, *Ann. Glaciol.*, 33, 221–224, doi:10.3189/172756401781818833.
- Perovich, D. K., and T. C. Grenfell (1981), Laboratory studies of the optical properties of young sea ice, *J. Glaciol.*, 27(96), 331–346.
- Perovich, D. K., T. C. Grenfell, B. Light, and P. V. Hobbs (2002), Seasonal evolution of the albedo of multiyear Arctic sea ice, *J. Geophys. Res.*, 107(C10), 8044, doi:10.1029/2000JC000438.
- Pierrehumbert, R. T., D. S. Abbot, A. Voigt, and D. Koll (2011), Climate of the Neoproterozoic, *Annu. Rev. Earth Planet. Sci.*, 39(1), 417–460, doi:10.1146/annurev-earth-040809-152447.
- Skiles, S. M. (2014), A method to retrieve the complex refractive index and single scattering optical properties of dust deposited in mountain snow, doctoral dissertation, Univ. of Calif. Los Angeles, Los Angeles.
- Stamnes, K., S. C. Tsay, W. Wiscombe, and K. Jayaweera (1988), Numerically stable algorithm for discrete-ordinate-method radiative transfer in multiple scattering and emitting layered media., *Appl. Opt.*, 27(12), 2502–2509, doi:10.1364/AO.27.002502.
- Toner, J. D., D. C. Catling, and B. Light (2014), The formation of supercooled brines, viscous liquids, and low-temperature perchlorate glasses in aqueous solutions relevant to Mars, *Icarus*, 233, 36–47, doi:10.1016/j.icarus.2014.01.018.
- Wagner, R., O. Möhler, and M. Schnaiter (2012), Infrared optical constants of crystalline sodium chloride dihydrate: Application to study the crystallization of aqueous sodium chloride solution droplets at low temperatures., *J. Phys. Chem. A*, 116(33), 8557–8571, doi:10.1021/jp306240s.
- Warren, S. G., and R. E. Brandt (2008), Optical constants of ice from the ultraviolet to the microwave: A revised compilation, *J. Geophys. Res.*, 113, D14220, doi:10.1029/2007JD009744.
- Wiscombe, W. J. (1980), Improved Mie scattering algorithms., *Appl. Opt.*, 19(9), 1505–1509.
- Wiscombe, W. J., R. M. Welch, and W. D. Hall (1984), The effects of very large drops on cloud absorption. Part I: Parcel models, *J. Atmos. Sci.*, 41(8), 1336–1355.
- Zatko, M. C., and S. G. Warren (2015), East Antarctic sea ice in spring: Spectral albedo of snow, nilas, frost flowers and slush, and light-absorbing impurities in snow, *Ann. Glaciol.*, 56(69), 53–64, doi:10.3189/2015AoG69A574.